Article

Graphene-Integrated Plasmonic Metamaterial for Manipulation of Multi-Band Absorption, Based on Near-Field Coupled Resonators

Man Hoai Nam [1,2], Bui Son Tung [1,2,*], Bui Xuan Khuyen [1,2,*], Duong Thi Ha [2,3], Nguyen Van Ngoc [1,2], Manh Cuong Tran [4] , Dac Tuyen Le [5], Vu Dinh Lam [2], Liangyao Chen [6], Haiyu Zheng [7,8] and YoungPak Lee [6,7,8,*]

[1] Institute of Materials Science, Vietnam Academy of Science and Technology, 18 Hoang Quoc Viet, Cau Giay, Hanoi 100000, Vietnam; nammh@ims.vast.ac.vn (M.H.N.); nguyenvanngoc182@gmail.com (N.V.N.)

[2] Graduate University of Science and Technology, Vietnam Academy of Science and Technology, 18 Hoang Quoc Viet, Hanoi 100000, Vietnam; hadt@tnue.edu.vn (D.T.H.); lamvd@gust-edu.vast.ac.vn (V.D.L.)

[3] Thai Nguyen University of Education, Thai Nguyen 250000, Vietnam

[4] Faculty of Physics, Hanoi National University of Education, 136 Xuan Thuy, Cau Giay, Hanoi 100000, Vietnam; tmcuong@hnue.edu.vn

[5] Department of Physics, Hanoi University of Mining and Geology, 18 Pho Vien, Hanoi 100000, Vietnam; ledactuyen@humg.edu.vn

[6] Department of Optical Science and Engineering, Fudan University, Shanghai 200433, China; lychen@fudan.ac.cn

[7] Quantum Photonic Science Research Center and RINS, Department of Physics, Hanyang University, Seoul 04763, Korea; haiyu@hanyang.ac.kr

[8] Alpha ADT Co., Ltd., Hwaseong 18469, Korea

* Correspondence: yplee@hanyang.ac.kr (Y.L.); tungbs@ims.vast.ac.vn (B.S.T.); khuyenbx@ims.vast.ac.vn (B.X.K.)

Abstract: We demonstrated a multi-band plasmonic metamaterial absorber (MA), based on the near-field coupled resonators. In addition to the individual resonances of resonators in the proposed structure, which were split-ring resonator (SRR) and cross-shape structures, another resonance was also excited owing to the coupling of resonators, revealing a triple-band absorption. Furthermore, to control the absorption behavior, on the top of the SRRs, the identical SRRs made of graphene ink were pasted. By increasing the resistance of graphene ink, the coupling strength was weakened, changing the triple-band absorption to a dual-band one. Our work might be useful as the controllable devices, based on graphene-integrated plasmonic MA, such as filters, detectors and energy harvesters.

Keywords: metamaterial; multi-band absorption; near-field coupling; graphene

1. Introduction

Metamaterial (MM) is an artificial material which plays an important role in the field of science and technology today. The MM is composed of resonance structures, the so-called "meta-atoms," whose sizes are many times smaller than the operating wavelength. By designing it reasonably, the MM can exhibit unusual properties which are not available in the constituent elements. Thanks to that, the unusual properties, such as the inversion of Snell's law [1], negative refractive index [2,3] and electromagnetic (EM)-wave absorption [4,5], are obtained easily. Therefore, the MM is promising for the potential applications such as sensors [6–8], superlens [9,10], filters [11,12], antennas [13,14], and so on.

Nowadays, EM-wave absorbing materials are receiving great attention from materials scientists around the world, due to many capabilities in both civilian and military domains. Metamaterial absorber (MA) was proposed firstly by Landy et al. in 2008 [4]. The MA can absorb the energy of EM impinging on the material surface. Compared with the traditional absorbing materials, the MA has the advantages of being thin, light, and easy to select the desired absorption frequency. Therefore, it can be integrated into compact devices easily and conveniently. However, the ability to control the absorption properties

of MA is still limited, because one resonance structure often works only at the fundamental absorption frequency. To overcome this obstacle, various strategies have been developed such as incorporating electronic turning components [15–17], microfluidics [18], micro-electromechanical systems (MEMS) [19,20], etc. These methods enable to manipulate effectively the perfect-absorption frequencies of MA. However, they require complicated and costly fabrication processes.

Recently, the tunable MA can be achieved by integrating external materials, including the use of graphene or graphene ink. Graphene is known as a monolayer of carbon atom arranged in a honeycomb structure., which performs novel properties such as high electron mobility, mechanical flexibility, and tunability. Therefore, graphene is one of the potential candidates for the tunable MA, especially, in the THz range [21–23]. In addition, the conductive inks based on graphene, which have advantages in term of flexibility, lightweight and low-cost mass production, are also exploited for the MA [24,25].

In this work, we have investigated and proposed a way to expand the absorption property of MA, operating in the GHz region but based on the near-field coupling of resonators. Furthermore, by integrating resistive graphene-ink into the MA, the absorption behavior can be also controlled. Our investigation aims at simple approaches to manipulate the absorption behavior in perfect MA. These results are intended to meet the necessary demands for civilian, including healthcare, and military applications.

2. Methods

The proposed MA unit cell is shown in Figure 1. The MA structure consisted of an FR-4 dielectric layer in between two copper layers. In our simulation, we took the permittivity of FR-4 to be 4.3 with a loss tangent of 0.025. Copper with a conductivity $\sigma = 5.8 \times 10^7$ S·m^{-1} was chosen for both top and bottom metallic layers. In this case, the bottom layer was made of a continuous copper plate while the top layer consisted of split-ring resonator (SRR) and cross-shape (CS) patterns. The detail parameters of plasmonic MA are presented in Table 1.
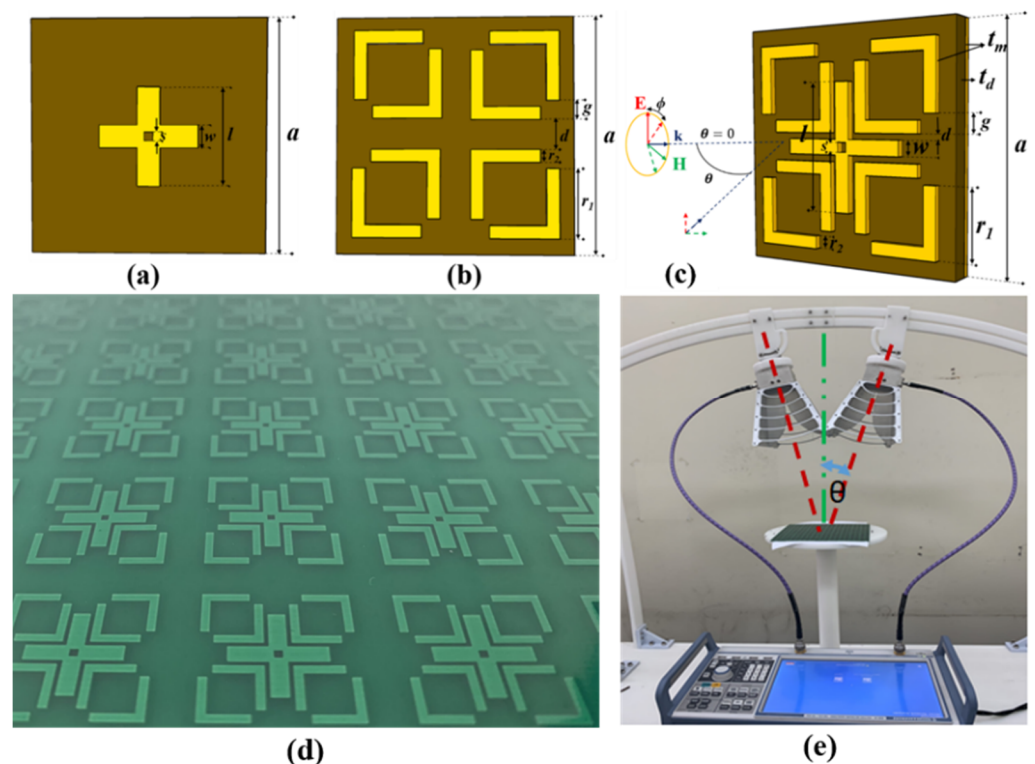
Figure 1. Unit-cell structure of the proposed MA: (**a**) CS structure, (**b**) SRR structure and (**c**) MA structure combined with two structures. (**d**) Fabricated MA sample and (**e**) measurement configuration.

Table 1. Structural parameters of the MA.

Parameter	a	d	g	l	r_1	r_2	s	t_d	t_m	w
Value (mm)	22	1	1.5	11	7	1	0.5	1.6	0.035	2

Simulation results were obtained by using the software CST Microwave Studio [26] based on the finite integration technique [27]. Frequency domain solver was used in a frequency range from 5.5 to 10.0 GHz. Since the bottom layer is a continuous metal plane, there is no wave passing through our structure. Therefore, the absorption of MA structure is calculated as

$$A(\omega) = 1 - |S_{11}(\omega)|^2 - |S_{21}(\omega)|^2 = 1 - |S_{11}(\omega)|^2 \tag{1}$$

where $S_{11}(\omega)$ and $S_{21}(\omega)$ are the reflection and transmission parameters, respectively.

In experiments, the MA sample, which is shown in Figure 1d, was fabricated by using the lithography technique including exposure, development, etching and removing processes. A vector network analyzer (VNA) ZNB20 attached to a pair of transmitter and receiver horn antennas was exploited to measure the reflection parameters of MA, as shown in Figure 1e. The distance between antenna and sample is approximately 2 m and the angle of incidence θ is about 15 degrees.

3. Results and Discussion

Figure 2 presents the simulated absorption spectra of the CS structure (Figure 2a), SRR one (Figure 2b), and the proposed MA structure combined with both ones (Figure 2d). The results point out that the absorption of CS structure reaches 98.4% at 6.85 GHz, while that of the SRR structure is 82.2% at 8.5 GHz. Although each individual structure gives only a single peak, by taking them together the proposed MA exhibits a 92.2% absorption peak at 6.85 GHz, and two close absorption ones at 8.37 and 8.65 GHz with absorption magnitude of 98% and 99.8%, respectively. These two absorption peaks form an absorption band with an absorption over 80% from 8.28 to 8.75 GHz. The results show that, besides the absorption peaks of the two individual structures, the coupling of resonators also generates a new resonance peak, showing the multi-band absorption spectrum of proposed plasmonic MA. The corresponding S_{11}, S_{21}, S_{22} and S_{12} parameters of MA are also plotted in Figure 2c, which show that the proposed MA absorbs only the wave incoming to the front structure layer, while the MA reflects totally the wave incoming to the back continuous metallic layer.

The influence of the distance d between CS and SRR structures on the absorption spectrum of MA was studied and is shown in Figure 3. Here, distance d was changed by fixing the position of CS and displacing the SRRs. The simulated results present that, when d decreases from 1 to 0.5 mm, there is a slight change at the first absorption resonance with a minor shift from 6.85 to 6.80 GHz. Meanwhile, two absorption peaks close to each other are changed clearly. Specifically, the absorption frequencies of second and third peaks move to 8.36 and 8.80 GHz, respectively, when d = 0.5 mm. Meanwhile, the absorption of second peak increases to be 99.4%, while that of the third peak decreases slightly to be 95%. The observation indicates that parameter d plays an important role in controlling the coupling of the two resonators. When d is smaller, the near-field coupling of SRR and CS is stronger, making the resonance peak separated further. The phenomenon is consistent with previously-published results on the near-field coupling (plasmonic) effect between resonance structures in MM [28–31]. From the obtained results, it can be concluded that by controlling the structural parameter d, the separation between absorption frequencies is changed. Thus, the absorption region from 8.28 to 8.75 GHz can be converted from a broadband (at a larger d) to a dual-band absorption (at a smaller d). The measured absorption spectra in Figure 3b are in a quite good agreement with the simulated ones in Figure 3a. Small deviations in the absorption frequency and magnitude might be due to the tolerance of fabricated samples. The influence of incident angle on the absorption spectrum of MA (d = 0.5 mm) is simulated and presented in Figure 3c. The result shows

that the absorption spectrum of MA is nearly unchanged for small incident angles. The absorption spectrum of MA is only significantly changed at larger incident angles, which are larger than 45 degrees. Therefore, it can be ensured that, in our experiment, the measured absorption of MA at small incident angles is similar to that at the normal incidence.
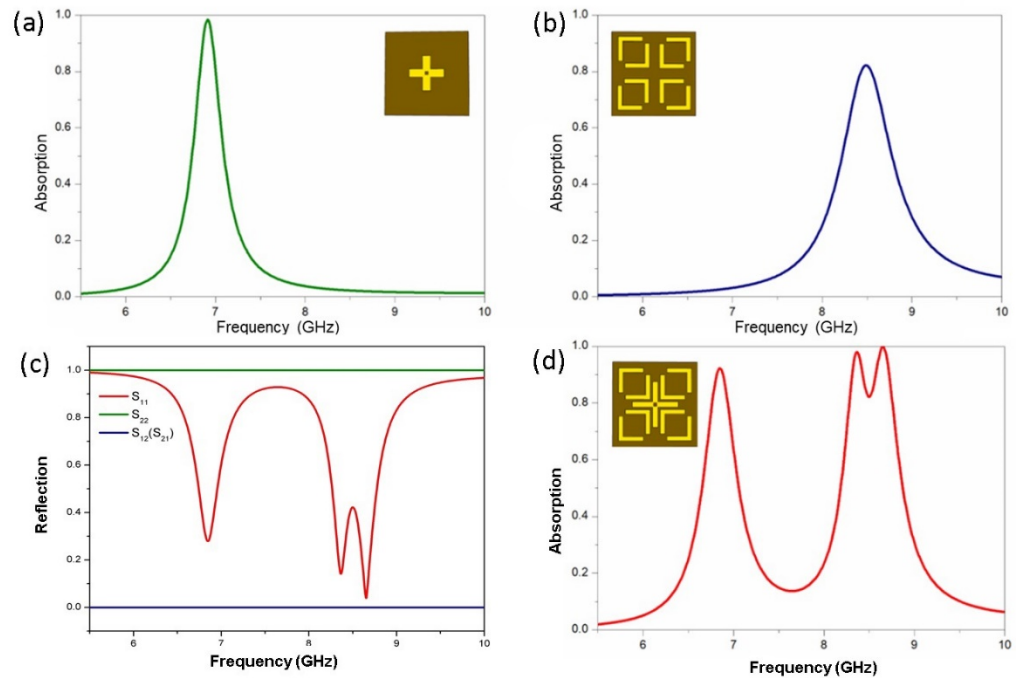
**Figure 2.** Absorption spectrum of (**a**) CS structure and (**b**) SRR one. (**c**) Parameters S_{11}, S_{22} and $S_{12}(S_{21})$, and (**d**) absorption spectrum of the proposed MA.
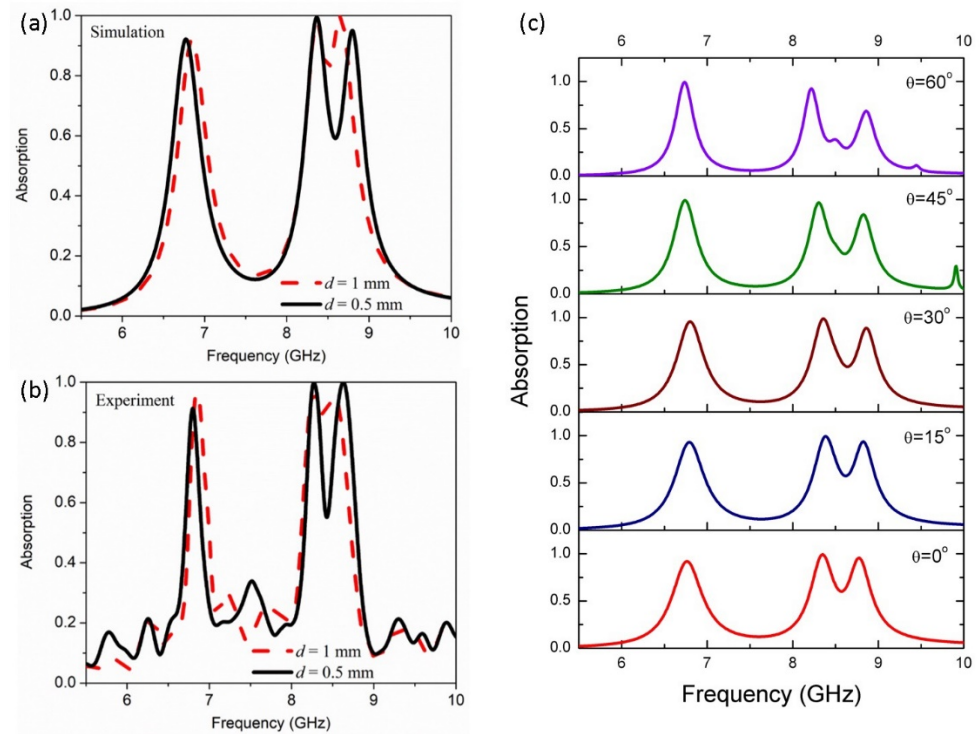
Figure 3. Dependences of (**a**) simulated and (**b**) measured absorption spectra on the distance d between SRR and CS structures and (**c**) dependence of the absorption spectrum on the incidence angle.

To clarify the mechanism of plasmonic MA, the surface-current distribution on the structure was simulated and is presented in Figure 4. It can be seen that all the resonances at absorption frequencies are the magnetic resonances caused by antiparallel induced surface currents on the top and bottom metallic layers. At 6.80 GHz, the induced current is concentrated mainly on the CS structure, meaning that the first absorption frequency is the individual resonance one of CS structure. Meanwhile, at 8.36 and 8.80 GHz, the induced currents are distributed mainly on the SRR, indicating the main role of SRRs at the second and the third absorption frequencies. However, the current distribution is not uniform on the SRR structure. The currents are located mainly on the outer branches of SRRs at 8.36 GHz, while those are excited strongly on the inner branches of SRRs at 8.80 GHz. The observed results show that the absorption resonances at 8.36 and 8.89 GHz are also affected by the coupling of SRR and CS structures, which redistributes the surface current on the SRR differently from the other frequency.
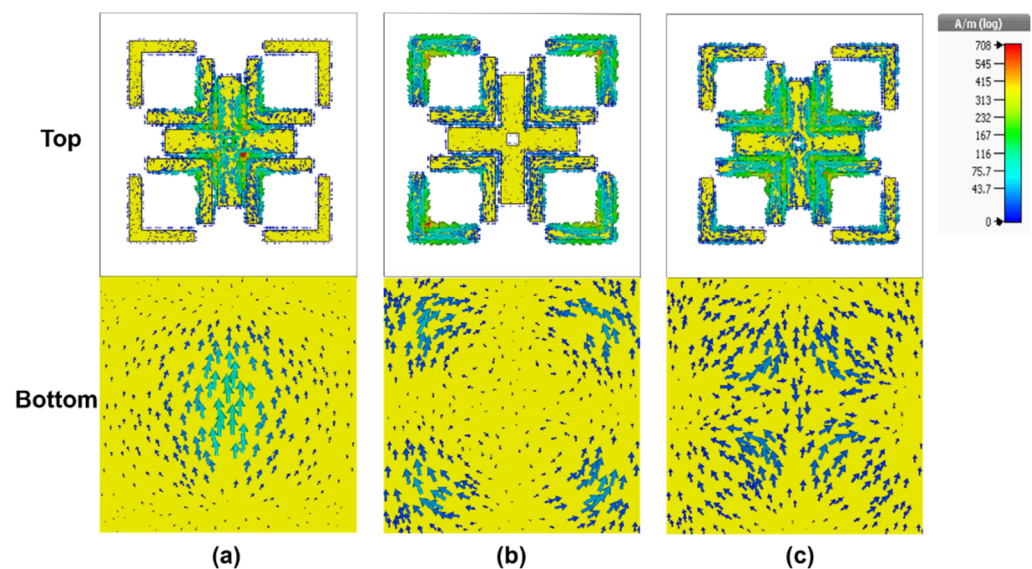

Figure 4. Surface-current distribution on the MA structure when *d* = 0.5 mm at absorption frequencies of (**a**) 6.80, (**b**) 8.36 and (**c**) 8.80 GHz.

In next investigation, we propose a simple way to manipulate the near-field coupling of resonators in the MA by exploiting graphene. Figure 5 illustrates the unit-cell configuration of graphene-integrated plasmonic MA. A graphene-ink was pasted on top of the SRRs of aforementioned MA (with *d* = 0.5 mm). To adjust the near-field coupling strength, different graphene inks were used with the resistance varied from 7.2 to 30 Ω/sq. The graphene sheet resistance was characterized based on the four-probe method by using the Helpass HPS2523 resistance tester (HELPASS, Changzhou, China).

Figure 6 shows the simulated and measured absorption spectra of bare MA and proposed graphene-integrated plasmonic one. In the simulation, when the sheet resistance of graphene ink is 7.2 Ω/sq, the first peak is nearly unchanged since the individual absorption resonance of CS structure is not affected by the graphene. However, the separation between second and third peaks is reduced gradually. At the same time, the absorption of these peaks decreases remarkably, broadening the absorption spectrum to be a frequency region from 8.26 to 8.86 GHz for an absorption range only from 70% to 80%. When the sheet resistance of graphene ink increases further from 7.2 to 30 Ω/sq, the first absorption peak is still nearly unchanged. On the other hand, the second and third peaks are transformed to be a single peak at 8.4 GHz and the absorption is reduced more to be roughly 60%.
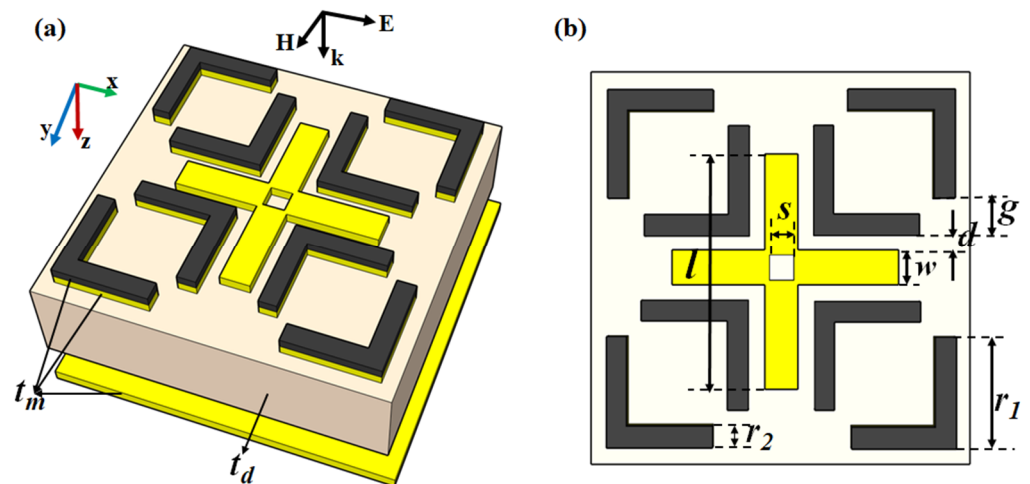
Figure 5. Unit-cell configuration of the graphene-integrated plasmonic MA in (**a**) perspective and (**b**) top views.
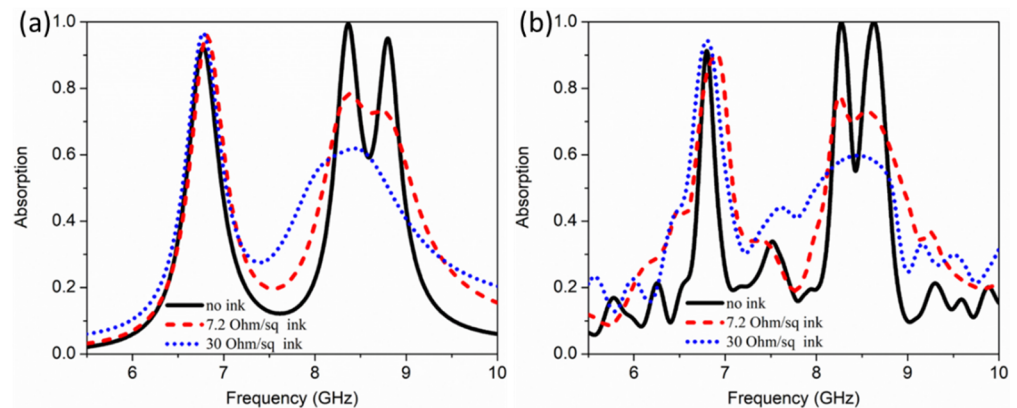
Figure 6. (**a**) Simulated and (**b**) experimental absorption spectra of bare and graphene-integrated plasmonic MAs with different resistances of graphene ink.

In the experiment, the measured absorption spectra show the similar behaviors as the simulated ones. The reduction of separation between second and third peaks, and the decrease of absorption can be explained, based on the resistance of graphene-ink. In the graphene-integrated plasmonic MA, the graphene layer acts as the resistive layer which weakens the strength of individual resonance of SRR. Consequently, the near-field coupling of SRR and CS resonators is also weakened, making the separation in frequency between second and third peaks is smaller. Furthermore, it is noteworthy that the resonance intensity of SRR is weaken by the resistive graphene layer. The change of resonance intensity alters the impedance of MA. Hence, the impedances of MA and air do not match anymore. Consequently, the absorption magnitude is decreased accordingly in the presence of graphene ink. Since both coupling of resonators and resonance strength of SRR decrease, not only these two peaks are transformed to a single peak, but the absorption is also reduced. The obtained results indicate that the absorption behavior of multi-band plasmonic MA can be controlled effectively by integrating the graphene ink into the MA structure.

To gain insight into the absorption mechanism of plasmonic MA, the distribution of surface current on the conductive parts of MA is simulated at distinct absorption frequencies. Figure 7a shows the surface current distributions at 6.80, 8.38 and 8.76 GHz of MA integrated with the graphene ink whose sheet resistance is 7.2 Ω/sq. Obviously, all of these resonances are the magnetic resonances caused by anti-parallel induced surface currents on the conductive layers. At 6.80 GHz, the induced current is still enhanced mainly around the CS structure. The induced currents at 8.38 GHz are concentrated on the outer edges of

SRRs. Meanwhile, at 8.76 GHz the induced currents are located mainly on the inner edges and partly at the outer ones of SRRs. In comparison with the surface-current distribution in Figure 4, the currents are not clearly distributed on the outer and inner edges at the second and third absorption peaks, respectively. This indicates that the coupling of resonators is weaker under the existence of resistive graphene ink. The simulated surface currents present that the resonance at 6.80 GHz is due to the magnetic response caused by the individual CS structure, while the absorption band from 8.26 to 8.86 GHz result from both individual magnetic responses of the SRR structure and weak coupling of the SRRs and CS. When the sheet resistance of graphene ink comes to be 30 Ω/sq, at 6.78 and 8.40 GHz, similarly the top and bottom surface currents are anti-parallel to each other, confirming that the absorption mechanism is affected by the magnetic resonance. Here, the induced current at 6.78 GHz is still built up mainly on the CS structure. However, at 8.40 GHz, the surface current distribution is uniform on the SRR. The observed phenomena indicate that the high resistance of graphene ink weakens the near-field coupling effect. Therefore, the coupling of resonators becomes less active and the absorption peak is contributed predominantly by the individual resonance of SRR structure.
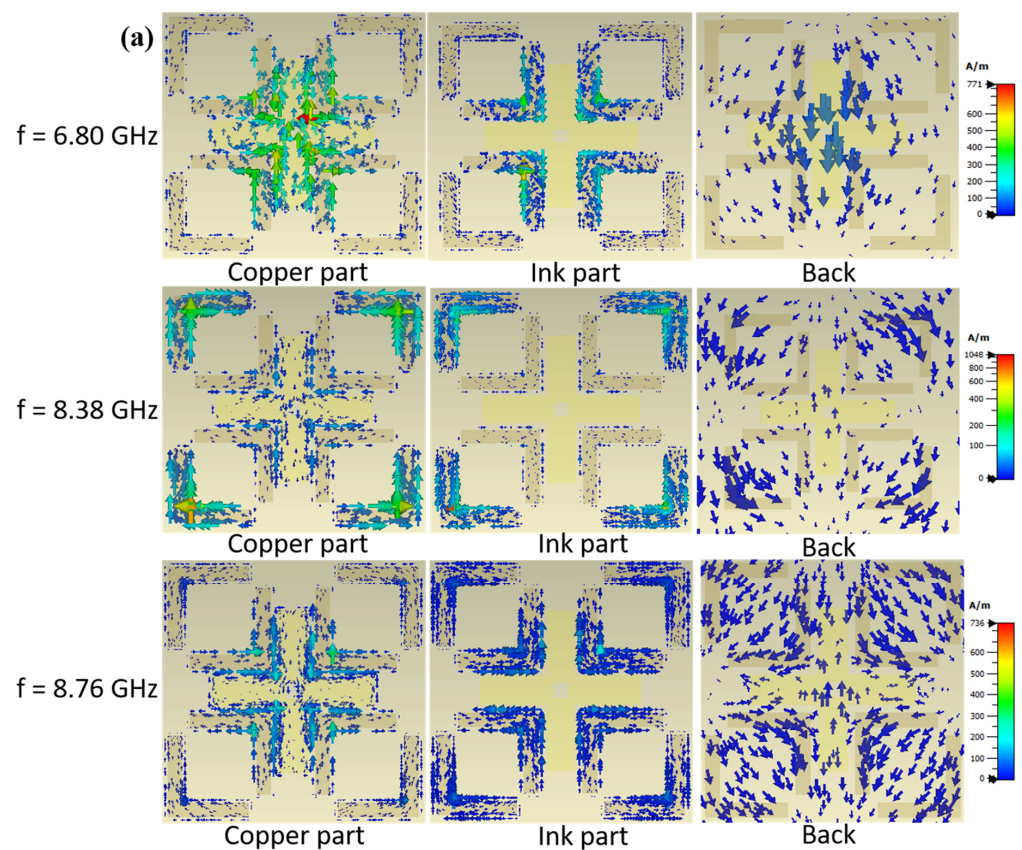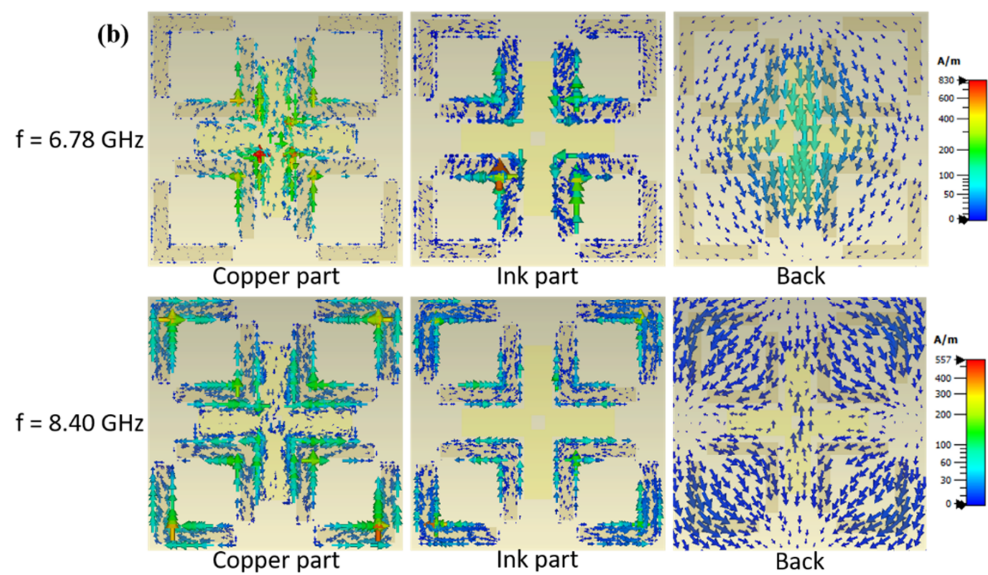

Figure 7. *Cont.*

Figure 7. Surface-current distribution with different sheet resistances of graphene ink: (**a**) 7.2 and (**b**) 30 Ω/sq.

4. Conclusions

In this paper, we have proposed and demonstrated a multi-band plasmonic MA operating in the GHz region (5.5–10 GHz), which is capable of changing the absorption characteristics, based on the near-field coupling of resonators and the graphene ink. Specifically, the plasmon MA exhibits the multi-band absorption at 6.80, 8.36 and 8.80 GHz with absorption of 92.2%, 99.4% and 95%, respectively, when the distance *d* between SRR and CS resonator is optimized to be 0.5 mm. The multi-band absorption is not only excited by the individual resonances but also the coupling of resonators. By changing the distance between SRR and CS resonators, the coupling effect is adjusted, which varies the separation between second and third absorption peaks. Then, by integrating graphene ink into the plasmonic MA, the absorption behavior is manipulated effectively. When the resistance of graphene ink is high with a value of 30 Ω/sq, both coupling of resonators and resonance strength of SRR structure is reduced, making the triple-band absorption is transformed to a dual-band absorption with the absorption deceasing to be about 60% at high frequency. Our research contributes a simple approach to control the absorption behavior of multi-band MA, which is potential for various plasmonic devices such as filters, gas-sensors/detectors and energy harvesters.

Author Contributions: M.H.N., B.S.T., B.X.K., V.D.L. and Y.L. conceived the idea. The electromagnetic simulation and calculation were carried out by D.T.H., B.S.T., B.X.K., N.V.N. and H.Z. The experiments were carried out by M.H.N., B.X.K., M.C.T. and D.T.L., M.H.N., B.S.T., B.X.K., L.C., Y.L. and V.D.L. analyzed and wrote the article. All of the authors discussed and commented on the manuscript. All authors have read and agreed to the published version of the manuscript.

Institutional Review Board Statement: Not applicable.

Informed Consent Statement: Not applicable.

Data Availability Statement: The data presented in this paper are available on request from the corresponding author.

Conflicts of Interest: The authors declare no conflict of interest. The funders had no role in the design of the study; in the collection, analyses, or interpretation of data; in the writing of the manuscript, or in the decision to publish the results.

References

1.　Ziolkowski, R.W. Pulsed and CW Gaussian beam interactions with double negative metamaterial slabs. *Opt. Express* **2003**, *11*, 662–681. [CrossRef] [PubMed]
2.　Veselago, V.G. The Electrodynamics of Substances with Simultaneously Negative Values of ϵ and μ. *Sov. Phys. Usp.* **1968**, *10*, 509–514. [CrossRef]
3.　Wang, J.; Allein, F.; Boechler, N.; Friend, J.; Vazquez-Mena, O. Design and fabrication of negative-refractive-index metamaterial unit cells for near-megahertz enhanced acoustic transmission in biomedical ultrasound applications. *Phys. Rev. Appl.* **2021**, *15*, 024025. [CrossRef]
4.　Landy, N.I.; Sajuyigbe, S.; Mock, J.J.; Smith, D.R.; Padilla, W.J. Perfect metamaterial absorber. *Phys. Rev. Lett.* **2008**, *100*, 207402. [CrossRef]
5.　Norouzi-Razani, A.; Rezaei, P. Broadband polarization insensitive and tunable terahertz metamaterial perfect absorber based on the graphene disk and square ribbon. *Results Phys.* **2022**, *34*, 105313. [CrossRef]
6.　Cong, L.; Tan, S.; Yahiaoui, R.; Yan, F.; Zhang, W.; Singh, R. Experimental demonstration of ultrasensitive sensing with terahertz metamaterial absorbers: A comparison with the metasurfaces. *Appl. Phys. Lett.* **2015**, *106*, 031107. [CrossRef]
7.　Bui, T.S.; Dao, T.D.; Dang, L.H.; Vu, L.D.; Ohi, A.; Nabatame, T.; Lee, Y.P.; Nagao, T.; Hoang, C.V. Metamaterial-enhanced vibrational absorption spectroscopy for the detection of protein molecules. *Sci. Rep.* **2016**, *6*, 32123. [CrossRef]
8.　Cao, Y.; Ruan, C.; Chen, K.; Zhang, X. Research on a high-sensitivity asymmetric metamaterial structure and its application as microwave sensor. *Sci. Rep.* **2022**, *12*, 1255. [CrossRef]
9.　Zhang, X.; Liu, Z. Superlenses to overcome the diffraction limit. *Nat. Mater.* **2008**, *7*, 435–441. [CrossRef]
10.　Dhama, R.; Yan, B.; Palego, C.; Wang, Z. Super-Resolution Imaging by Dielectric Superlenses: TiO$_2$ Metamaterial Superlens versus BaTiO$_3$ Superlens. *Photonics* **2021**, *8*, 222. [CrossRef]
11.　Nagarajan, A.; Erve, K.V.; Gerini, G. Ultra-narrowband polarization insensitive transmission filter using a coupled dielectric-metal metasurface. *Opt. Express* **2020**, *28*, 773–787. [CrossRef] [PubMed]
12.　Shan, S.; Wen, F.; Cheng, L. Purified nonlinear guided waves through a metamaterial filter for inspection of material microstructural changes. *Smart Mater. Struct.* **2021**, *30*, 095017. [CrossRef]
13.　Dietlein, C.; Luukanen, A.; Popovic, Z.; Grossman, E. A W-band polarization converter and isolator. *IEEE Trans. Antennas Propag.* **2007**, *55*, 1804–1809. [CrossRef]
14.　Olan-Nuñez, K.N.; Murphy-Arteaga, R.S. A novel metamaterial-based antenna for on-chip applications for the 72.5–81 GHz frequency range. *Sci. Rep.* **2022**, *12*, 1699. [CrossRef] [PubMed]
15.　Wu, T.; Li, W.; Chen, S.; Guan, J. Wideband frequency tunable metamaterial absorber by splicing multiple tuning ranges. *Results Phys.* **2021**, *20*, 103753. [CrossRef]
16.　Tennant, A.; Chambers, B. A single-layer tuneable microwave absorber using an active FSS. *IEEE Microw. Wirel. Compon. Lett.* **2004**, *14*, 46–47. [CrossRef]
17.　Xu, W.; Sonkusale, S. Microwave diode switchable metamaterial reflector/absorber. *Appl. Phys. Lett.* **2013**, *103*, 031902. [CrossRef]
18.　Ling, K.; Yoo, M.; Su, W.; Kim, K.; Cook, B.; Tentzeris, M.M.; Lim, S. Microfluidic tunable inkjet-printed metamaterial absorber on paper. *Opt. Express* **2015**, *23*, 110. [CrossRef]
19.　Bilgin, H.; Zahertar, S.; Sadeghzadeh, S.; Yalcinkaya, A.D.; Torun, H. A MEMS-based terahertz detector with metamaterial-based absorber and optical interferometric readout. *Sens. Actuator A Phys.* **2016**, *244*, 292–298. [CrossRef]
20.　Li, T.Y.; Wang, L.; Wang, J.M.; Li, S.; He, X.J. A dual band polarization-insensitive tunable absorber based on terahertz MEMS metamaterial. *Integr. Ferroelectr.* **2014**, *151*, 157–163. [CrossRef]
21.　Kakenov, N.; Balci, O.; Takan, T.; Ozkan, V.A.; Altan, H.; Kocabas, C. Observation of gate-tunable coherent perfect absorption of terahertz radiation in graphene. *ACS Photonics* **2016**, *3*, 1531–1535. [CrossRef]
22.　Liu, M.; Cheng, W.; Zhang, Y.; Zhang, H.; Zhang, Y.; Li, D. Multi-controlled broadband terahertz absorber engineered with VO 2-integrated borophene metamaterials. *Opt. Mater. Express* **2021**, *11*, 2627–2638. [CrossRef]
23.　Qi, L.; Liu, C. Broadband multilayer graphene metamaterial absorbers. *Opt. Mater. Express* **2019**, *9*, 1298–1309. [CrossRef]
24.　Long, L.V.; Khiem, N.S.; Tung, B.S.; Tung, N.T.; Giang, T.T.; Son, P.T.; Khuyen, B.X.; Lam, V.D.; Chen, L.; Zheng, H.; et al. Flexible Broadband Metamaterial Perfect Absorber Based on Graphene-Conductive Inks. *Photonics* **2021**, *8*, 440. [CrossRef]
25.　Pan, K.; Leng, T.; Song, J.; Ji, C.; Zhang, J.; Li, J.; Hu, Z. Controlled reduction of graphene oxide laminate and its applications for ultra-wideband microwave absorption. *Carbon* **2020**, *160*, 307–316. [CrossRef]
26.　CST Microwave Studio 2015, License ID: 52856-1. Dassault Systèmes. Available online: http://www.cst.com (accessed on 28 February 2022).
27.　Weiland, T. A discretization model for the solution of Maxwell's equations for six-component fields. *Arch. Elektron. Übertrag.* **1977**, *31*, 116–120.
28.　Bai, R.; Zhang, C.; Gu, X.; Jin, X.R. Unidirectional reflectionlessness and perfect nonreciprocal absorption in stacked asymmetric metamaterial based on near-field coupling. *Appl. Phys. Express* **2017**, *10*, 112001. [CrossRef]
29.　Pham, T.L.; Dinh, H.T.; Le, D.H.; Bui, X.K.; Bui, S.T.; Dang, H.L.; Phan, A.D.; Le, D.T.; Vu, D.L. Dual-band isotropic metamaterial absorber based on near-field interaction in the Ku band. *Curr. Appl. Phys.* **2020**, *20*, 331–336. [CrossRef]

30. Tung, B.S.; Khuyen, B.X.; Kim, Y.J.; Lam, V.D.; Kim, K.W.; Lee, Y.P. Polarization-independent, wide-incident-angle and dual-band perfect absorption, based on near-field coupling in a symmetric metamaterial. *Sci. Rep.* **2017**, *7*, 11507. [CrossRef]
31. Tung, B.S.; Khuyen, B.X.; Kim, Y.J.; Hwang, J.S.; Lam, V.D.; Chen, L.-Y.; Lee, Y.P. Manipulation of the near-field coupling in metamaterial for multi-band absorber. *Waves Random Complex Media* **2021**, *31*, 2290–2300. [CrossRef]